European Journal of Mechanics B/Fluids 47 (2014) 57–67

Contents lists available at ScienceDirect

European Journal of Mechanics B/Fluids

journal homepage: www.elsevier.com/locate/ejmflu

Onset of convection in a porous layer with continuous periodic horizontal stratification, Part II: Three-dimensional convection

D.A.S. Rees [a], A. Barletta [b,*]

[a] Department of Mechanical Engineering, University of Bath, Claverton Down, Bath BA2 7AY, UK

[b] Department of Industrial Engineering, Alma Mater Studiorum Università di Bologna, Viale Risorgimento 2, Bologna 40136, Italy

ARTICLE INFO

Article history:
Available online 17 February 2014

Keywords:
Porous medium
Linear stability
Horizontal layer
Heterogeneity
Nonuniform permeability
Floquet theory

ABSTRACT

The onset of convection in a porous layer which is heated from below is considered. In particular we seek to determine the effect of spatially periodic variations in the permeability field on the identity of the onset mode as a function of both the period P of this variation and its amplitude A. A Floquet theory is assumed in order to ensure that the analysis is as general as possible. It is found that convection is always three-dimensional and that the critical Rayleigh number always decreases as either the period or the amplitude of the permeability variation increases. Furthermore, the corresponding Floquet exponent ν is either 0 or 1, and the range of values of P over which $\nu = 1$ corresponds to the favoured mode has been obtained as a function of A.

1. Introduction

The onset of convective instability in a porous layer with a vertical temperature gradient has been the subject of very considerable attention particularly in the course of the last few decades. The first studies on this topic [1,2] were formulations of the classical Rayleigh–Bénard problem within the context of filtration processes in porous media as modelled through Darcy's law [3]. A development of these early studies on what might be called the Darcy–Bénard problem, was carried out by Palm et al. [4] in order to investigate the nonlinear effects under slightly supercritical conditions. These authors obtained an expression for the Nusselt number to high order in the supercritical parameter $(Ra - Ra_c)/Ra$, where Ra is the Rayleigh number and $Ra_c = 4\pi^2$ is its critical value at the onset of instability [3].

While there are many different extensions that one might apply to the Darcy–Bénard problems, some of which are the adoption of Brinkman and/or inertia effects, the dropping of the assumption of local thermal nonequilibrium, and the consideration of inclined layers or ones which conducting boundaries, the one which we concentrate on here is the effect of a heterogeneous permeability field. Heterogeneity could comprise layered materials or media where the permeability varies continuously with one or more coordinates, or else it could be random. McKibbin and O'Sullivan [5] studied a horizontally layered material and showed that large permeability differences are required for the multilayered medium to display onset conditions markedly different from those for a homogeneous layer. This analysis was developed further by Rees and Riley [6] by taking into account weakly nonlinear effects and they showed that double or multiple minimum loci for the Rayleigh number may exist at onset of instability. Studies of the Darcy–Bénard problem for heterogeneous porous media were carried out also by Nield and Simmons [7]. We mention that other sensible developments on this topic were achieved by McKibbin [8] and by Nield [9].

A situation where the permeability undergoes a periodic change was envisaged by De Wit and Homsy [10,11]. However, the kind of instability investigated by these authors is definitely different from the buoyancy-induced Rayleigh–Bénard instability. In fact, the physical effect leading to the instability is a concentration-dependent viscosity in the binary fluid saturating the porous medium. Much more closely related to the present paper is the work of Rees and Tyvand [12] (hereinafter referred to as Part 1) who considered a porous layer with a permeability which varies periodically in a horizontal direction. The analysis carried out in that paper was two-dimensional thus limiting the study to the behaviour of transverse rolls, i.e. ones with axes that are perpendicular to the direction of the x-axis along which the permeability changes periodically.

The aim of this contribution is to extend the investigation reported by Rees and Tyvand [12] from two-dimensional to three-dimensional modes. The Floquet theory, which was employed by

* Corresponding author. Tel.: +39 051 2093287.
E-mail addresses: D.A.S.Rees@bath.ac.uk (D.A.S. Rees), antonio.barletta@unibo.it (A. Barletta).

http://dx.doi.org/10.1016/j.euromechflu.2014.02.008
0997-7546/

Rees and Tyvand [12] to determine the selected two-dimensional modes of instability, is used in this study in order to determine whether two-dimensional modes or three-dimensional modes are favoured at onset of convection.

2. Governing equations

We consider a plane porous layer saturated by a Newtonian fluid. The thickness of the layer is H. The boundary planes at $z = 0$ and $z = H$ are impermeable and isothermal, and are held at the temperatures T_h and T_c, respectively, where $T_h > T_c$. The permeability, K, varies periodically in the x-direction and satisfies the following trigonometrical law,

$$K = K_0 \left[1 + A\cos(\lambda x/H)\right], \tag{1}$$

where K_0 is the mean permeability, $A \in [0, 1)$ is a dimensionless amplitude, and λ is a dimensionless wavenumber which is such that $2\pi H/\lambda$ is the period of the permeability distribution (see Fig. 1).

The onset of convection in the porous layer is carried out under the following assumptions: (i) Darcy's law holds; (ii) the Oberbeck–Boussinesq approximation may be applied; (iii) the effective thermal conductivity and the effective volumetric heat capacity (the average product of the density and the specific heat) of the saturated porous medium are approximately uniform; (iv) there is local thermal equilibrium between the solid phase and the fluid phase; (v) no internal heating effect occurs. Assumption (iii) is a realistic description of porous media with an approximately uniform porosity. In spite of that, permeability can still be non-uniform. For instance, this may be the case with beds of particles or fibres, where the permeability may be inhomogeneous with a homogeneous porosity due to a variable morphology as, say, a spatially-varying average particle or fibre diameter. Another argument is that, while the effective thermal conductivity and the effective volumetric heat capacity depend on the porosity, permeability is controlled by the interconnected porosity of the medium. The latter parameter excludes from the evaluation of the void volume fraction the dead-end pores, where the fluid cannot actually flow.

We can express the governing equations in a dimensionless form by adopting the scalings,

$$\begin{aligned} &\frac{1}{H}(x, y, z) \to (x, y, z), \qquad \frac{\alpha_m}{\sigma H^2}\, t \to t, \\ &\frac{H}{\alpha_m}(u, v, w) \to (u, v, w), \\ &\frac{T - T_c}{T_h - T_c} \to T, \qquad \frac{K_0 H}{\mu\alpha_m}\, \nabla p \to \nabla p. \end{aligned} \tag{2}$$

Here, x, y, z and t denote the Cartesian coordinates and time, u, v, w are the velocity components, T is the temperature, ∇p is the dynamic pressure gradient, α_m is the effective thermal diffusivity of the saturated porous medium, μ is the fluid viscosity, and σ is the ratio between the effective volumetric heat capacity of the saturated porous medium and the volumetric heat capacity (the product of the density and the specific heat) of the fluid.

On account of Eq. (2), the dimensionless local balance equations for mass, momentum and heat transport may be written as

$$\frac{\partial u}{\partial x} + \frac{\partial v}{\partial y} + \frac{\partial w}{\partial z} = 0, \tag{3a}$$

$$u = -F(x)\,\frac{\partial p}{\partial x}, \qquad v = -F(x)\,\frac{\partial p}{\partial y}, \qquad w = -F(x)\left(\frac{\partial p}{\partial z} - Ra\,T\right), \tag{3b}$$

$$\nabla^2 T = \frac{\partial T}{\partial t} + u\,\frac{\partial T}{\partial x} + v\,\frac{\partial T}{\partial y} + w\,\frac{\partial T}{\partial z}, \tag{3c}$$

while the boundary conditions are expressed as

$$\begin{aligned} &z = 0: \qquad w = 0, \qquad T = 1, \qquad \frac{\partial p}{\partial z} = Ra, \\ &z = 1: \qquad w = 0, \qquad T = 0, \qquad \frac{\partial p}{\partial z} = 0. \end{aligned} \tag{4}$$

Here, $F(x)$ and the Darcy–Rayleigh number Ra are defined respectively as,

$$F(x) = 1 + A\cos(\lambda x), \qquad Ra = \frac{\rho_c g\beta\,(T_h - T_c)\,K_0 H}{\mu\alpha_m}, \tag{5}$$

where ρ_c is the fluid density at the reference temperature T_c, g is the modulus of the gravitational acceleration $\mathbf{g}$, and β is the thermal expansion coefficient of the fluid.

The aim of this paper is to understand how the onset of three-dimensional convection depends on the values of the non-dimensional parameters, A, P and ν, where A is the amplitude of the permeability variation, $P = 2\pi/\lambda$ is the period of that variation, and ν is the Floquet exponent to be introduced below.

3. Basic solution and analysis of linear disturbances

A basic state which is a stationary solution of Eqs. (3) and (4) with a zero velocity exists and is given by

$$\begin{aligned} &u_b = v_b = w_b = 0, \qquad T_b = 1 - z, \qquad \frac{\partial p_b}{\partial x} = 0, \\ &\frac{\partial p_b}{\partial y} = 0, \qquad \frac{\partial p_b}{\partial z} = Ra\,(1 - z), \end{aligned} \tag{6}$$

where the subscript b denotes the "basic solution". We introduce small-amplitude disturbances of the basic solution, Eq. (6), as follows,

$$\begin{aligned} &(u, v, w) = (u_b, v_b, w_b) + \varepsilon\,(U, V, W), \qquad T = T_b + \varepsilon\theta, \\ &\nabla p = \nabla p_b + \varepsilon\nabla\mathcal{P}, \end{aligned} \tag{7}$$

where ε is a perturbation parameter, such that $|\varepsilon| \ll 1$. We now substitute Eqs. (6) and (7) into Eqs. (3) and (4), and neglect terms which are of $O(\varepsilon^2)$. Thus, the system of linearised disturbance equations is given by

$$\frac{\partial U}{\partial x} + \frac{\partial V}{\partial y} + \frac{\partial W}{\partial z} = 0, \tag{8a}$$

$$U = -F(x)\,\frac{\partial \mathcal{P}}{\partial x}, \qquad V = -F(x)\,\frac{\partial \mathcal{P}}{\partial y}, \qquad W = -F(x)\left(\frac{\partial \mathcal{P}}{\partial z} - Ra\,\theta\right), \tag{8b}$$

$$\nabla^2\theta = \frac{\partial\theta}{\partial t} - W, \tag{8c}$$

$$z = 0, 1: \qquad W = 0, \qquad \theta = 0. \tag{8d}$$

A pressure–temperature formulation is obtained by substituting Eq. (8b) into Eq. (8a), so that we finally obtain

$$\nabla^2\mathcal{P} = Ra\,\frac{\partial\theta}{\partial z} - G(x)\,\frac{\partial\mathcal{P}}{\partial x}, \tag{9a}$$

$$\nabla^2\theta = \frac{\partial\theta}{\partial t} + F(x)\left(\frac{\partial\mathcal{P}}{\partial z} - Ra\,\theta\right), \tag{9b}$$

$$z = 0, 1: \qquad \frac{\partial\mathcal{P}}{\partial z} = 0, \qquad \theta = 0, \tag{9c}$$

where

$$G(x) = \frac{F'(x)}{F(x)} = -\frac{A\lambda\sin(\lambda x)}{1 + A\cos(\lambda x)}, \tag{10}$$

and where the prime denotes an ordinary derivative with respect to x.

Eqs. (9) may be solved as an eigenvalue problem which defines the marginal stability condition for the Darcy–Rayleigh number Ra. However, there is a natural periodicity in the x-direction which is caused by the permeability variations, and this is not necessarily one which will yield the smallest value of the critical Rayleigh number. Therefore we may use Floquet theory to attempt to maximise the range of available disturbances that may be considered. Therefore we may write $\mathcal{P}$ and θ as

$$\mathcal{P}(x,y,z,t) = \mathfrak{Re}\{Raf(x)e^{i(ky+\lambda\nu x/2-\omega t)}\}\cos(\pi z), \tag{11a}$$

$$\theta(x,y,z,t) = \mathfrak{Re}\{h(x)e^{i(ky+\lambda\nu x/2-\omega t)}\}\sin(\pi z), \tag{11b}$$

where k is the wavenumber, ω is a temporal frequency and ν is the Floquet exponent. All three of these parameters are real provided that marginal stability is considered. Substitution of Eq. (11) into Eqs. (9) yields

$$\left(f'' + i\lambda\nu f' - \tfrac{1}{4}\lambda^2\nu^2 f\right) + G(x)\left(f' + \tfrac{1}{2}i\lambda\nu f\right) - \left(k^2+\pi^2\right)f - \pi h = 0, \tag{12a}$$

$$\left(h'' + i\lambda\nu h' - \tfrac{1}{4}\lambda^2\nu^2 h\right) - \left[k^2+\pi^2 - i\omega\right]h + Ra\,F(x)\,(h+\pi f) = 0. \tag{12b}$$

These equations are then solved subject to the periodicity conditions,

$$f(0) = f(P), \qquad f'(0) = f'(P), \qquad h(0) = h(P), \qquad h'(0) = h'(P), \tag{13}$$

as an eigenvalue problem for Ra in terms of A, P, ν and the spanwise wavenumber, k. The aim then is to minimise Ra with respect to both ν and k. The principle of exchange of stabilities applies to Eqs. (12) and (13) (see Appendix A) and therefore we may set $\omega = 0$. We also mention that the two-dimensional problem which was investigated by Rees and Tyvand [12] is obtained from that defined by Eq. (12) in the limit $k \to 0$, i.e. when the disturbances become independent of y.

The eigenvalue problem given by Eqs. (12) and (13) was solved using precisely the same numerical scheme that was devised in Rees and Tyvand [12] and described there in great detail. Briefly, the two ordinary differential equations were approximated using an eighth-order finite difference method where the resulting difference equations were rearranged into the form of a matrix eigenvalue problem for Ra. With such a high order method, numerical accuracy of at least six significant figures could be obtained with a relatively small number of grid points. In general we used 40 intervals per unit distance. Accuracy of encoding the method was provided by a comparison with solutions obtained using a fourth-order Runge–Kutta scheme coupled with a shooting method. Neutral curves, some of which will be presented below, generally provided a single minimum. This minimum was found by means of a Newton–Raphson scheme applied to five values of Ra which were obtained for five closely-spaced values of k. Thus, if we write $Ra = Ra(k)$, then we require those values of k for which $dRa/dk = 0$. Thus corrections in k are given by the standard formula,

$$\delta k = -Ra'(k)/Ra''(k), \tag{14}$$

where the following fourth-order central difference approximations are used to approximate the above derivatives,

$$Ra'(k) \simeq \left[\tfrac{1}{12}Ra(k-2\epsilon) - \tfrac{2}{3}Ra(k-\epsilon) + \tfrac{2}{3}Ra(k+\epsilon) - \tfrac{1}{12}Ra(k+2\epsilon)\right]/\epsilon, \tag{15a}$$

$$Ra''(k) \simeq \left[-\tfrac{1}{12}Ra(k-2\epsilon) + \tfrac{4}{3}Ra(k-\epsilon) - \tfrac{5}{2}Ra(k) + \tfrac{4}{3}Ra(k+\epsilon) - \tfrac{1}{12}Ra(k+2\epsilon)\right]/\epsilon^2. \tag{15b}$$

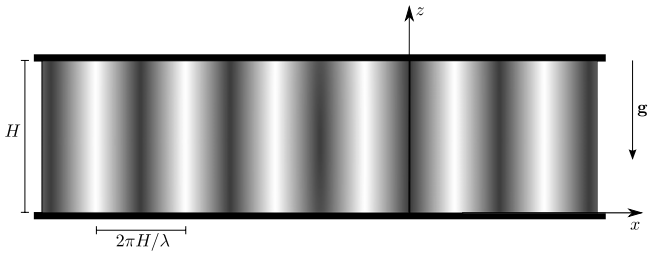

Fig. 1. The fluid-saturated porous layer with a periodic horizontal permeability field.

Minimisation using these approximations yielded at least three if not more than four figures of accuracy even when ϵ is as large as 0.01, which is well in excess of what is required for graphical resolution.

4. Discussion of the results

4.1. Mode shapes

Before we present details of the neutral curves and the minimisation of the critical values of Ra over k and ν, it is important to have an idea about what the computed solutions look like. While the present computations are one-dimensional, the onset modes are three-dimensional, but the mode shapes themselves are visualised easily by plotting contours of the rate of heat transfer at either the upper or lower surfaces of the layer, and this yields a two-dimensional view of how the disturbance varies with x and y.

Fig. 2 compares onset modes for the two amplitudes, $A = 0.1$ and $A = 0.3$, for the four cases, $P = 0.5$, $P = 1$, $P = 2$ and $P = 4$. We have selected $k = \pi$ as a representative wavenumber, and have set $\nu = 0$ so that the onset modes have the same periodicity in the x-direction as the permeability variation. All the plots are confined to the region $0 \le x \le 4$ and $0 \le y \le 2$ for easy comparison, and the values of P are such that the patterns in this Figure tessellate the plane.

When both A and P take small values, then the resulting pattern takes the form of longitudinal rolls at leading order, with small-amplitude variations about this state; this is evident for the case $A = 0.1$ and $P = 0.5$ where the effect of permeability changes is only just visible. As the period increases, then the onset mode becomes increasingly confined to those regions where the permeability takes its largest value. When the amplitude of the permeability variation takes larger values, then the localisation of the convection pattern becomes more extreme because the local Rayleigh number (i.e. one which is based on permeability at the currently chosen value of x) varies much more greatly over a period. But once the period of the variation is sufficiently large, there is little visual difference between the mode shapes for small and large values of A, although larger values of A give profiles which are slightly more concentrated towards the permeability maxima.

Changes in the value of the wavenumber, k, causes the width of the pattern in the y-direction to change, as one expects, and therefore it is deemed not necessary to demonstrate this. However, it is an *a priori* expectation that non-zero values of the Floquet exponent could provide the most unstable mode for some choices of A and P. Therefore Fig. 3 shows how different values of ν affect the planform of the onset mode. This figure takes the case $A = 0.3$, $P = 2$ and $k = \pi$, where $0 \le x \le 8$ and $0 \le y \le 4$, i.e. four periods of the permeability variation and two spanwise periods are displayed.

When $\nu = 0$ we obtain the type of pattern shown in Fig. 2 where the longitudinal pattern is still quite evident even though there is much localisation in the regions of high permeability. When $\nu = 1$,

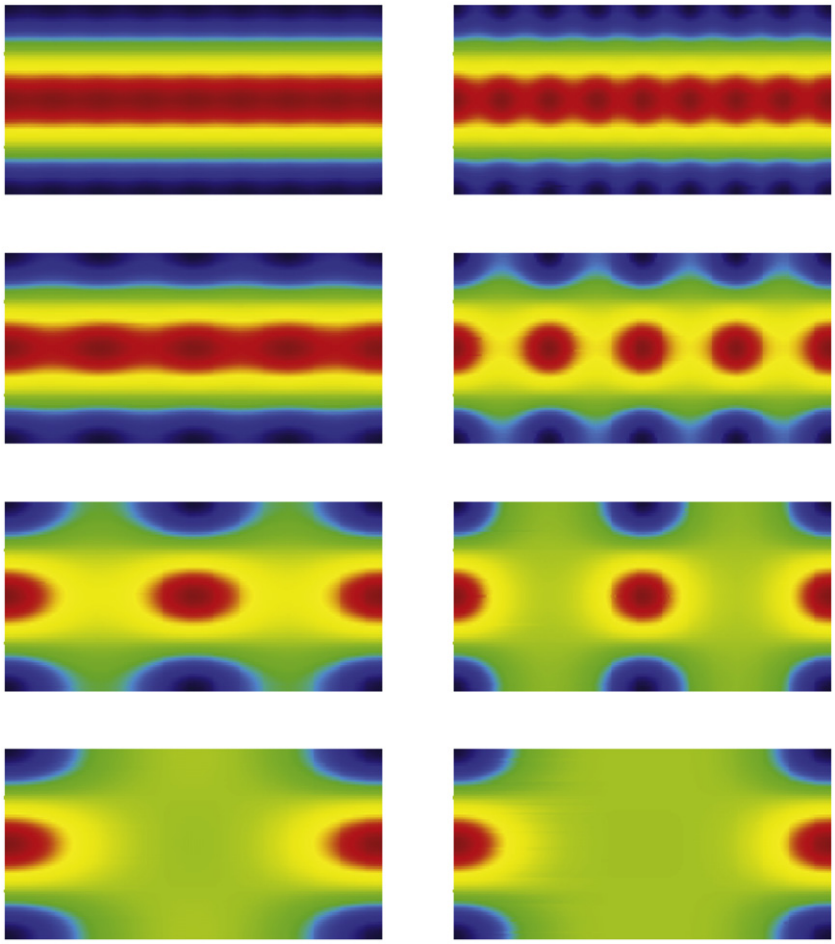

Fig. 2. Showing the lower surface rate of heat transfer for different onset modes for $A = 0.1$ (left) and $A = 0.3$ (right), and for $P = 0.5$ (uppermost), 1, 2 and 4 (lowest). Here $k = \pi$ and $\nu = 0$ and the shown patterns are confined to $0 \le x \le 4$ and $0 \le y \le 2$.

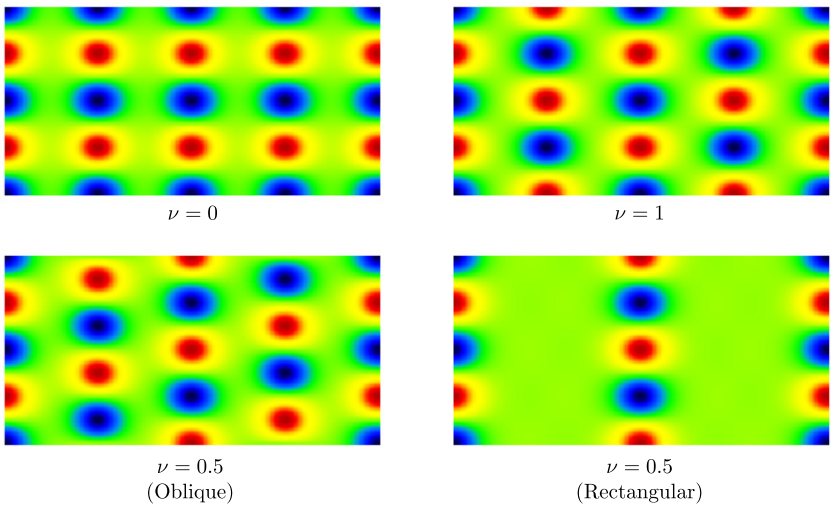

Fig. 3. Showing the lower surface rate of heat transfer for different onset modes for the case, $P = 2$, $A = 0.3$ and $k = \pi$, and for the values of ν shown.

regions of positive and negative rates of heat transfer alternate as x increases, and the overall pattern has a period of $2P = 4$ in the x-direction. When $\nu = 0.5$, we show two different forms of the onset mode. The pattern which is labelled, *Oblique*, is the natural pattern which arises due to the substitution which is given in Eq. (11). The line of, say, red spots is aligned at an angle to the x-axis and could be said to form an oblique mode. There is, of course, a second form of this which is equivalent to $\nu = -0.5$, but graphically it may be seen by turning the present plot upside-down. A third form is obtained by adding the two different oblique modes together. This has the effect of removing almost completely any disturbance in alternating regions of high permeability; this

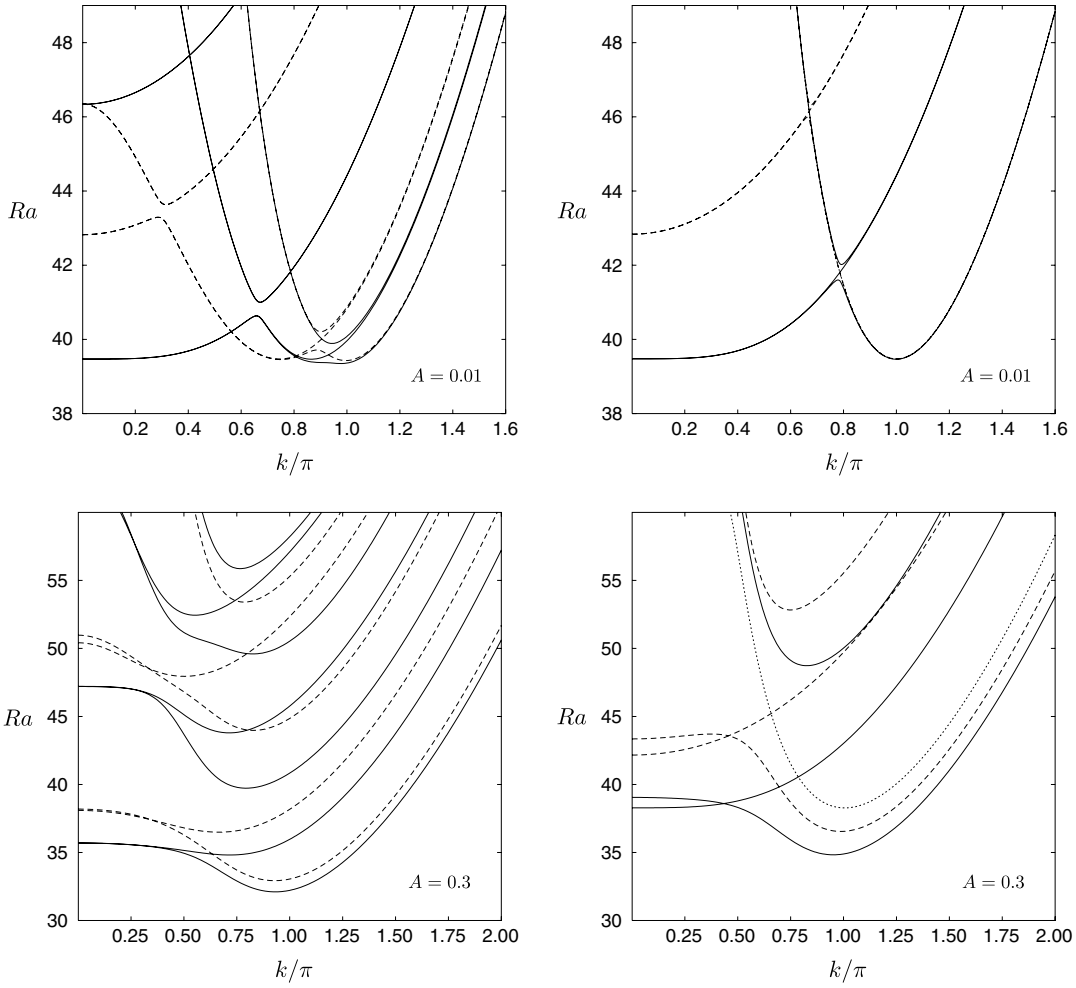

Fig. 4. Showing how neutral curves vary with P for $A = 0.1$ and $A = 0.3$. Here $\nu = 0$. In the two left hand frames continuous lines depict $P = 4$ and dashed lines $P = 3$. In the right hand frames continuous lines depict $P = 2$, dashed lines $P = 1.5$ and dotted lines $P = 1$. Up to six modes are displayed.

is the one labelled as *Rectangular* in Fig. 3. The period of each of these three patterns is now $4P = 8$. Other more complicated patterns may be obtained, but these are not shown in the interests of brevity. All of these modes will be referred to below as even modes because the patterns obey the same symmetry as that of the underlying permeability variation.

4.2. Neutral curves

In this subsection we attempt to convey a comprehensive understanding of how the neutral curves vary with the parameters, P, A and ν. While there are only three parameters to vary, this understanding is made more difficult to present than was expected *a priori* because neutral curves corresponding to distinct modes sometimes cross one another. This may be seen in Fig. 4 which displays the neutral curves corresponding to various modes for $A = 0.01$ and $A = 0.3$ and for $P = 1$, 1.5, 2, 3, and 4. The value $\nu = 0$ was taken here.

When $k \ll 1$ the first mode to appear is an odd one in x, which means that a dividing (or zero) disturbance isotherm arises at $x = 0$ and multiples of $x = P$, and therefore a transverse convection cell is centred precisely where the permeability is at its largest. These may be seen in Part 1. The second mode is one for which the temperature field is even in x, as shown in Figs. 2 and 3. When either P is sufficiently large or A sufficiently small, the values of Ra for these two modes are almost identical and are indistinguishable graphically. As k increases, the even mode takes over as the one which corresponds to the lower value of Ra. A clear transition of this kind is seen for the case, $A = 0.3$ and $P \leq 2$, which is shown in Fig. 4, and it is true for all other cases. For any chosen pair of values of A and P the minimum value of Ra (i.e. the critical Rayleigh number, Ra_c) corresponds to a mode which is even in x in general, and given that k is non-zero, it is also a longitudinal roll. Thus we have already settled the fact that transverse (or two-dimensional rolls) never form the most unstable mode.

When $A = 0.01$ the shapes of the neutral curves are seen to depend quite strongly on the period, P. However, the profile of the onset mode can change quite substantially as k increases from zero. If one focuses on the case, $A = 0.01$ and $P = 4$, then the onset mode for very small values of k is roughly proportional to $\sin \pi x$, i.e. it is an odd mode. As k increases, this changes suddenly to the corresponding even mode, $\cos \pi x$, as discussed above. The value of Ra then rises, reaches a maximum and decreases once more. In this region the mode changes gradually to one where the profile has only one minimum and one maximum in the period, P, and although it begins by having both signs, it eventually becomes a single-signed function of x.

Fig. 5 concentrates on the neutral curves corresponding to the onset mode, and therefore some curves display a discontinuous change of slope which reflects the crossing of two curves. Here we concentrate on the effect of different values of P on the onset criterion for both $A = 0.1$ and $A = 0.3$, with $\nu = 0$. While it is clear that the critical Rayleigh number is a decreasing function of P, the value of Ra close to $k = 0$ is not a monotonic function of P. This is

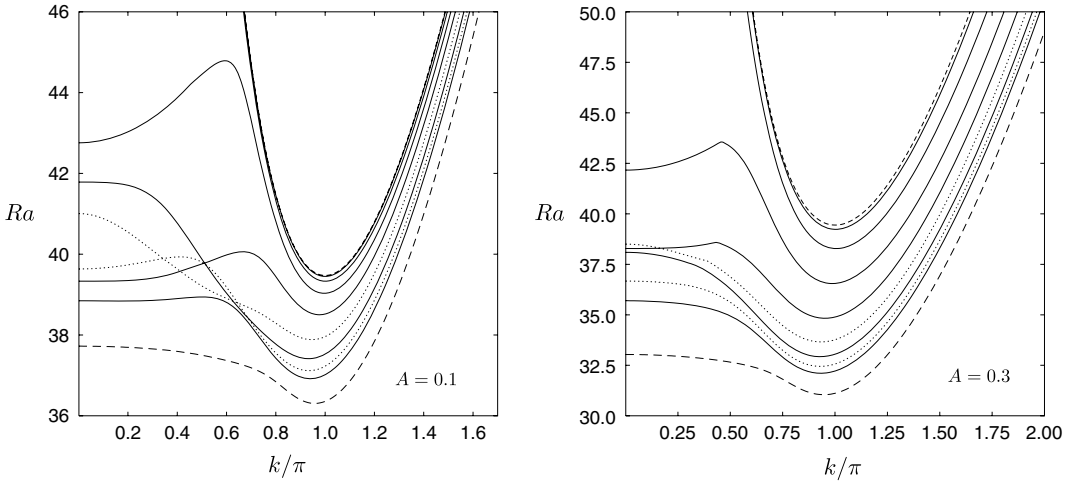

Fig. 5. Showing the neutral curves corresponding to the first mode for $P = 0.2$ (short dashes), 0.5, 1, 1.5, 2, 2.5, 3, 3.5, 4 and 8 (long dashes). Curves corresponding to $P = 2.5$ and 3.5 are dotted. Here $A = 0.1$ (left frame) and $A = 0.3$ (right frame) with $\nu = 0$.

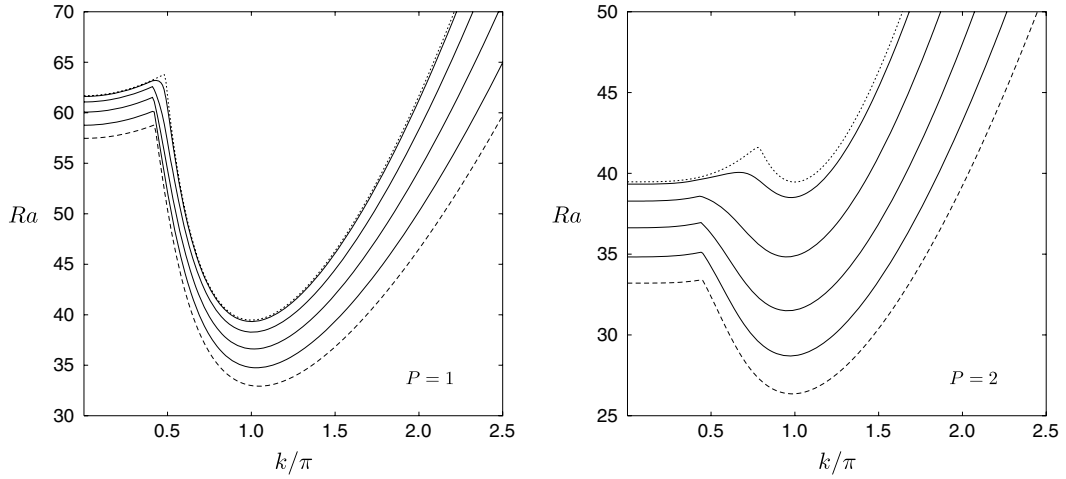

Fig. 6. Showing the neutral curves corresponding to the first mode for $A = 0.01$ (short dashes), 0.1, 0.3, 0.5, 0.7 and 0.9 (long dashes). Here $P = 1$ (left frame) and $P = 2$ (right frame) with $\nu = 0$.

caused by the difficulty of fitting cells, which would naturally have a wavelength of 2 into the period of the permeability variations. Indeed, Part 1 shows that this is achieved only by selecting non-zero values of ν to allow an appropriate spatial period of the onset profile. When P takes small values, the neutral curve is almost identical to that for the uniform porous layer, and the profile of the onset mode is generally very similar to that given in Fig. 2 for $P = 0.5$, i.e. it is a longitudinal vortex with short wavelength ripples.

Fig. 6 is concerned with how the amplitude, A, affects the onset criterion when $P = 1$ and $P = 2$. The manner in which the shapes of the neutral curves change with A is much more straightforward than how they change with P. The critical value, Ra_c, is a decreasing function of A in general. This is because of the presence of regions of permeability which are higher than the mean value that used to define the Rayleigh number.

The effect of varying ν is shown in Fig. 7 for $A = 0.3$ and for the two periods, $P = 0.8$ and $P = 2$. When $P = 0.8$ it is clear that the smallest value of Ra_c is obtained when $\nu = 0$, but when $P = 2$ it is $\nu = 1$. In Part 1 it was found that the minimising value of ν for two-dimensional convection varies smoothly between $\nu = 0$ and $\nu = 1$ and back. For three-dimensional convection we find that the transitions are always sudden, and that they arise for all amplitudes, A. These graphs also suggest that Ra_c varies monotonically with ν, which is actually not true in general. For a chosen value of A, there is a transitional value of P where $\nu = 1$ takes over from $\nu = 0$ as the minimising value. In such cases Ra_c increases from its $\nu = 0$ value to a maximum and then it decreases again towards its $\nu = 1$ value. Thus the transition in terms of ν is always discontinuous.

4.3. Critical values

All of this is summarised in Fig. 8 which displays the variation in Ra_c and k_c with P for a wide selection of values of A ranging from 0.01 to 0.9. First of all, we note that this figure confirms that Ra_c is a decreasing function of both A and P in all cases. Second, Ra_c appears to tend towards $4\pi^2$ when $P \to 0$ independently of the value of A; this feature is analysed in Appendix B and shows that the small-P limit yields an effectively isotropic medium. Third, the region in between the two black circles for each Ra_c curve is the region in which $\nu = 1$ comprises the most unstable mode. There appears only to be one such region; values of P which are outside of this range correspond to $\nu = 0$. The $\nu = 0$ curve, when it does not form the most unstable mode, is shown as a dotted line in this graph.

The corresponding wavenumbers are also shown. There is a tendency for $k \to \pi$ as $P \to 0$ (see Appendix B) and as $P \to \infty$ (see Appendix C). Somewhat surprisingly the value of k_c is quite

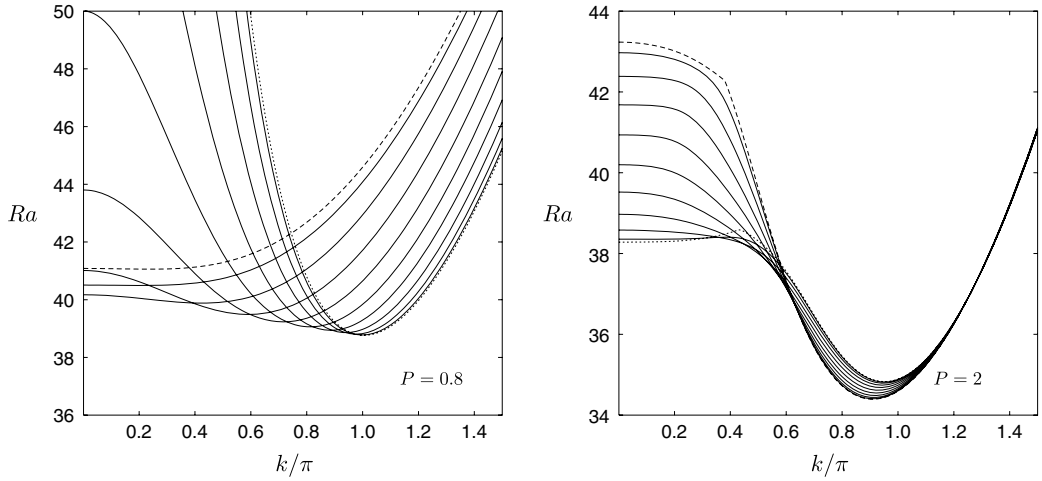

Fig. 7. Showing variation with ν of the neutral curves corresponding to the first mode for $A = 0.3$. The left frame corresponds to $P = 0.8$ and the right to $P = 2$. Dotted lines correspond to $\nu = 0$ and dashed lines to $\nu = 1$. The values of ν are separated by an increment of 0.1.

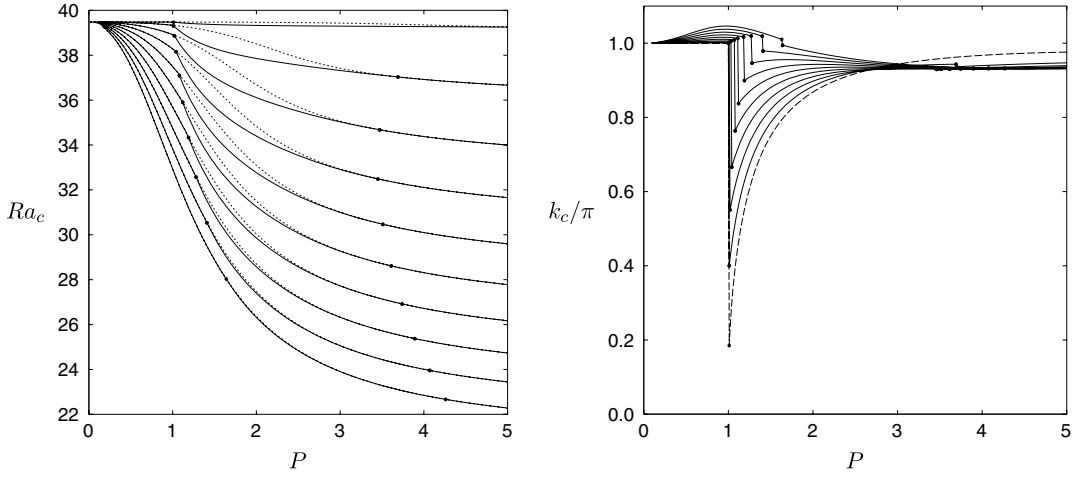

Fig. 8. Showing the variation of the critical values of Ra_c (left) and k_c (right) with P for $A = 0.01, 0.1, 0.2, 0.3\,(0.1)\,0.9$. For each Ra_c curve the two filled circles delineate the range of P over which $\nu = 1$ yields the smallest value of Ra_c, while $\nu = 0$ elsewhere. For Ra_c the uppermost line corresponds to $A = 0.01$; for k_c it is the dashed line.

small on the $\nu = 1$ side of the first transition when A is small. Such a mode looks more like a transverse roll with a relatively slow modulation in the y-direction but with a wavenumber roughly equal to π in the x-direction. This happens because $P = 1$ together with $\nu = 1$ yields a potential pattern in the x-direction which has a period of 2. Although it is tempting to cite this as a potential reason for having $\nu = 1$ solutions being favoured near to $P = 1$, it does not explain why the range of P over which $\nu = 1$ is favoured is so large.

The locus of points where the favoured mode makes its transition between $\nu = 0$ and $\nu = 1$ is shown in Fig. 9. The numerical values of P corresponding to the lower branch tend towards 1 as $A \to 0$, and therefore $\nu = 0$ forms the favoured mode whenever $P < 1$ for all amplitudes, A. With regard to the upper branch, the values of P appear to increase without bound as $A \to 0$, and it appears to satisfy a relation which is approximately of the form, $P \sim 1.74A^{-1/4}$. When $A = 0.001$ then $P = 9.5760$ on the upper branch.

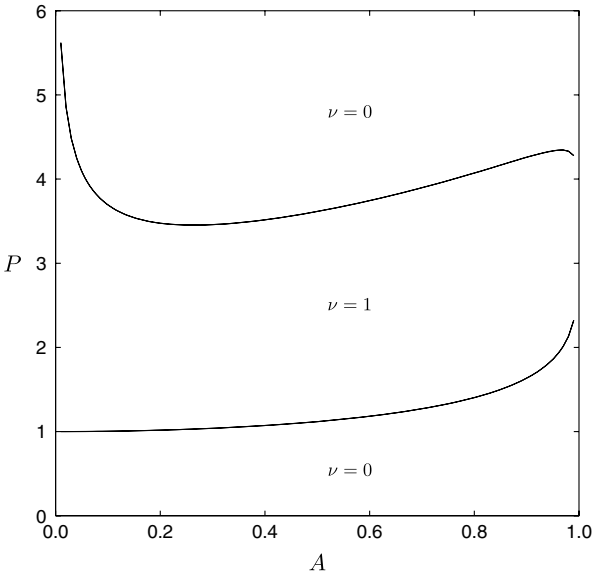

Fig. 9. Showing the regions in (A, P)-space in which either $\nu = 0$ or $\nu = 1$ forms the favoured onset mode.

5. Conclusions

This paper is a natural extension of the two-dimensional analysis of Part 1 into three dimensions. We have considered the effect of spatially periodic variations in the permeability on the onset of

convection in an otherwise uniform horizontal porous layer heated from below. When convection is confined to be two-dimensional, the critical parameters for the onset of convection were found in Part 1 to depend not only on the period and the amplitude of the permeability variations but also on the Floquet exponent. For example, the Floquet exponent corresponding to the most unstable mode changes continuously as the period of the variations change. In the present paper it has been shown that, when convection is allowed to be three-dimensional, the Floquet exponent only ever changes discontinuously as P increases from zero, and it does this only twice, namely from $\nu = 0$ to $\nu = 1$ when P takes a value which is a little greater than 1, and then a second time back to $\nu = 0$ at a value of P which is much more strongly dependent on the value of A. It is also found that the critical Rayleigh number always decreases as either P increases or A increases.

Appendix A. Exchange of stabilities

This analysis proceeds by first multiplying Eq. (12a) by $F\exp(i\lambda\nu x/2)$, and Eq. (12b) by $\exp(i\lambda\nu x/2)$ and rearranging them thus:

$$\left(Ff'e^{i\lambda\nu x/2}\right)' + \tfrac{i\lambda\nu}{2}\left(Ffe^{i\lambda\nu x/2}\right)' - (k^2+\pi^2)Ffe^{i\lambda\nu x/2} - \pi Fhe^{i\lambda\nu x/2} = 0, \tag{A.1a}$$

$$\left(h'e^{i\lambda\nu x/2}\right)' + \tfrac{i\lambda\nu}{2}\left(he^{i\lambda\nu x/2}\right)' - (k^2+\pi^2-i\omega)he^{i\lambda\nu x/2} + Ra\,F(h+\pi f)e^{i\lambda\nu x/2} = 0. \tag{A.1b}$$

These equations are now multiplied by the functions, $\bar{f}\exp(-i\lambda\nu x/2)$ and $\bar{h}\exp(-i\lambda\nu x/2)$, respectively, and integrated over one period, P. This is a legitimate step to take because the integrands of both integrals have precisely this period. The resulting equations may be added together in such a way that an integral involving $Fh\bar{f}$ is removed, and we thereby obtain,

$$\begin{aligned} i\omega\int_0^P |h|^2\,dx = \int_0^P \Big[&|h'|^2 + \left(k^2+\pi^2+\tfrac{1}{4}\lambda^2\nu^2 - Ra\,F\right)|h|^2 \\ &+ \frac{i\lambda\nu}{2}\left(h\bar{h}' - h'\bar{h}\right)\Big]dx \\ &+ Ra\int_0^P F\Big[|f'|^2 + \left(k^2+\pi^2+\tfrac{1}{4}\lambda^2\nu^2\right)|f|^2 \\ &+ \frac{i\lambda\nu}{2}\left(f\bar{f}' - f'\bar{f}\right)\Big]dx. \end{aligned} \tag{A.2}$$

All the terms on the right hand side of this equation are real, while the left hand side is purely imaginary. Therefore this equation may be satisfied if and only if $\omega = 0$. We therefore conclude that the principle of exchange of stabilities holds for all values of the given parameters, and that the onset problem is stationary.

Appendix B. Small-P analysis

For the sake of completeness we quote Eqs. (12a) and (12b) with $\nu = 0$:

$$Ff'' + F'f' - F\left(k^2+\pi^2\right)f - \pi Fh = 0, \tag{B.1a}$$

$$h'' - \left(k^2+\pi^2\right)h + Ra\,F(h+\pi f) = 0, \tag{B.1b}$$

where Eq. (12a) has been multiplied by F for later convenience, and where $F(x) = 1 + A\cos\lambda x$, $F'(x) = -A\lambda\sin\lambda x$ and $\lambda = 2\pi/P$.

We are interested in studying the small-P limit for $\nu = 0$. Fig. 8 suggests that $Ra_c \to 4\pi^2$ and $k_c \to \pi$ as $P \to 0$, where the approach to these limits is quadratic in P in both cases. A detailed examination of the modal shapes shows that both f and h tend towards being constants, despite potentially large variations in $F(x)$ when A is large.

The analysis begins by rescaling x, as follows,

$$\xi = \lambda x, \tag{B.2}$$

where $\lambda = 2\pi/P \gg 1$, and therefore Eqs. (B.1a) and (B.1b) become,

$$\lambda^2(F\ddot{f} + \dot{F}\dot{f}) - F\left(k^2+\pi^2\right)f - \pi Fh = 0, \tag{B.3a}$$

$$\lambda^2\ddot{h} - \left(k^2+\pi^2\right)h + Ra\,F(h+\pi f) = 0, \tag{B.3b}$$

where dots denote ordinary derivatives with respect to ξ, and $F = 1 + A\cos\xi$. The analysis now proceeds by expanding all quantities in series comprised of inverse powers of λ^2, and by insisting that solutions have period 2π in ξ:

$$(f, h, Ra) = (f_0, h_0, Ra_0) + \lambda^{-2}(f_1, h_1, Ra_1) + \lambda^{-4}(f_2, h_2, Ra_2) + \cdots. \tag{B.4}$$

At leading order we obtain the following equations,

$$F\ddot{f}_0 + \dot{F}\dot{f}_0 = 0, \qquad \ddot{h}_0 = 0, \tag{B.5}$$

from which we deduce that h_0 must be a constant. Although it is possible to obtain a periodic solution for f_0, the numerical evidence suggests that we should let f_0 take a constant value. These values will be set later.

At $O(\lambda^{-2})$ we obtain,

$$F\ddot{f}_1 + \dot{F}\dot{f}_1 = F\left(k^2+\pi^2\right)f_0 + \pi Fh_0, \tag{B.6a}$$

$$\ddot{h}_1 = \left(k^2+\pi^2\right)h_0 - Ra_0\,F(h_0+\pi f_0). \tag{B.6b}$$

Eq. (B.6b) may be written in the form,

$$\ddot{h}_1 = \left(k^2+\pi^2\right)h_0 - Ra_0\,(h_0+\pi f_0) - Ra_0\,A\cos\xi\,(h_0+\pi f_0),$$

and given that solutions must be periodic, then the constant terms on the right hand side must cancel. Therefore we find that,

$$Ra_0 = \frac{(k^2+\pi^2)h_0}{h_0+\pi f_0}, \tag{B.7}$$

and

$$h_1 = Ra_0\,A\cos\xi\,(h_0+\pi f_0). \tag{B.8}$$

We also need to apply the periodicity condition to the solution of Eq. (B.6a). In this case the coefficients of F on the right hand side need to sum to zero. This leads to the following expression relating the constant, f_0 and h_0,

$$\pi h_0 = -(k^2+\pi^2)f_0. \tag{B.9}$$

The actual magnitudes of f_0 and h_0 are no consequence because this is a linear theory, but we may set,

$$f_0 = -\pi \quad \text{and} \quad h_0 = k^2+\pi^2, \tag{B.10}$$

for convenience. This leads to,

$$Ra_0 = \frac{(k^2+\pi^2)^2}{k^2}, \tag{B.11}$$

as the leading order value of the Rayleigh number, which is confirmed in Fig. 8. We also note that Eq. (B.6a) now leads us to deduce that f_1 is a constant, but its value is obtained by imposing the need for periodic solutions at the next order.

At $O(\lambda^{-4})$ the equations for f_2 and h_2 are,

$$F\ddot{f}_2 + \dot{F}\dot{f}_2 = F\left(k^2+\pi^2\right)f_1 + \pi Fh_1, \tag{B.12a}$$

$$\ddot{h}_2 = \left(k^2+\pi^2\right)h_1 - Ra_0\,F(h_1+\pi f_1) - Ra_1\,F(h_0+\pi f_0). \tag{B.12b}$$

Table 1
Comparison between the numerical critical data and the two-term asymptotic formulae given in Eq. (B.18).

A	P	Ra_c/π^2		k_c/π	
		Num	Asymp	Num	Asymp
0.2	0.3	3.996248	3.9964	1.000447	1.000450
0.2	0.2	3.998370	3.9984	1.000200	1.000200
0.2	0.1	3.999598	3.9996	1.000050	1.000050
0.5	0.3	3.976862	3.9775	1.002774	1.002813
0.5	0.2	3.989871	3.9900	1.001243	1.001250
0.5	0.1	3.997492	3.9975	1.000312	1.000313
0.9	0.3	3.927594	3.9271	1.008786	1.009113
0.9	0.2	3.967683	3.9676	1.003996	1.004050

We follow the same procedure, namely to eliminate the possibility of secular growth and insist on having periodic solutions. Details of this analysis are omitted for the sake of brevity, but the chief outcomes are the following,

$$f_1 = -\tfrac{1}{2}\pi(k^2+\pi^2)A^2 \quad \text{and} \quad Ra_1 = -\frac{(k^2+\pi^2)^3}{2k^2}A^2. \tag{B.13}$$

Finally it is necessary to minimise Ra with respect to k. We have,

$$Ra = \frac{(k^2+\pi^2)^2}{k^2} - \frac{(k^2+\pi^2)^3}{2k^2}A^2\lambda^{-2} + O(\lambda^{-4}). \tag{B.14}$$

Clearly the minimising value of k will be close to π, given the form of the leading term and the fact that $\lambda \gg 1$. If we set $k^2 = \pi^2(1+\lambda^{-2}c)$ in Eq. (B.14), where c is a constant to be found, then we obtain,

$$Ra = \pi^2\Big(4 + c^2\lambda^{-4} + \cdots\Big) - \tfrac{1}{2}A^2\pi^4\Big(8 + 4c\lambda^{-2} + \cdots\Big)\lambda^{-2} + \Big[\text{constant} + O(\lambda^{-2})\Big]\lambda^{-4} + \cdots. \tag{B.15}$$

Although we have not computed the $O(\lambda^{-4})$ term in Ra, it will be a constant at leading order, and, apart from the determination of this constant, Eq. (B.15) is accurate to $O(\lambda^{-4})$. This expression for Ra may be written as,

$$Ra = 4\pi^2 - 4A^2\pi^4\lambda^{-2} + \Big[\pi^2 c(c - 2A^2\pi^2) + \text{constant}\Big]\lambda^{-4} + \cdots. \tag{B.16}$$

The $O(\lambda^{-4})$ coefficient is minimised when $c = A^2\pi^2$. From this we may now deduce that the leading two terms in the expressions for the critical Rayleigh number and wavenumber are,

$$\begin{aligned} Ra_c/\pi^2 &= 4 - 4A^2\pi^2\lambda^{-2} + O(\lambda^{-4}),\\ k_c/\pi &= 1 + \tfrac{1}{2}A^2\pi^2\lambda^{-2} + O(\lambda^{-4}). \end{aligned} \tag{B.17}$$

Given that $\lambda = 2\pi/P$, we may rewrite the above in terms of P:

$$\begin{aligned} Ra_c/\pi^2 &= 4 - P^2A^2 + O(P^4),\\ k_c/\pi &= 1 + \tfrac{1}{8}A^2P^2 + O(P^4). \end{aligned} \tag{B.18}$$

Comparisons between some of our computations and these asymptotic formulae are given in Table 1, and are seen to provide very good estimates, even when P is as large as 0.3.

Appendix C. Large-P analysis

Once more we quote Eqs. (12a) and (12b):

$$f'' + (F'/F)f' - \left(k^2+\pi^2\right)f - \pi h = 0, \tag{C.1a}$$

$$h'' - \left(k^2+\pi^2\right)h + Ra\,F(h+\pi f) = 0, \tag{C.1b}$$

where $F = 1 + A\cos\lambda x$ and $F' = -A\lambda\sin\lambda x$. Given that $\lambda = 2\pi/P$ the following analysis is undertaken as an asymptotic analysis for $\lambda \ll 1$. When $P \gg 1$ the onset modes tend to be centred on the regions of relatively high permeability and therefore we shall concentrate on the region near to $x = 0$. Given the analysis of the effect of long wavelength thermal modulations on Darcy–Bénard convection of Rees [13] the *a priori* expectation is for the onset mode to be governed by a fourth-order form of the parabolic cylinder equation. Therefore the following scaling for x was found:

$$\xi = \lambda^{1/3}x \tag{C.2}$$

in Eqs. (C.1a) and (C.1b). For the sake of convenience in the following analysis it is necessary to introduce the extra substitution,

$$k^2 = \alpha\pi^2. \tag{C.3}$$

Eqs. (C.1a) and (C.1b) now become,

$$\pi^2(1+\alpha)f + \pi h = \lambda^{2/3}\ddot{f} - \lambda^2\frac{A\xi}{1+A}\dot{f} + o(\lambda^2), \tag{C.4a}$$

$$\begin{aligned} &Ra(1+A)(h+\pi f) - \pi^2(1+\alpha)h\\ &\quad = -\lambda^{2/3}\ddot{h} + \tfrac{1}{2}\lambda^{4/3}Ra\,A\xi^2(h+\pi f) + o(\lambda^2). \end{aligned} \tag{C.4b}$$

In these equations the dots represent derivatives with respect to ξ. Solutions are now expanded in powers of $\lambda^{2/3}$, as follows; let

$$\begin{aligned} (f,h,\alpha,Ra) &= (f_0,h_0,\alpha_0,Ra_0) + (f_1,h_1,\alpha_1,Ra_1)\lambda^{2/3}\\ &\quad + (f_2,h_2,\alpha_2,Ra_2)\lambda^{4/3} + \cdots. \end{aligned} \tag{C.5}$$

At $O(1)$ we obtain,

$$\pi^2(1+\alpha_0)f_0 + \pi h_0 = 0, \tag{C.6a}$$

$$Ra_0(1+A)(h_0+\pi f_0) - \pi^2(1+\alpha_0)h_0 = 0. \tag{C.6b}$$

The solution of this pair of equations are assumed to be functions of ξ, and therefore we obtain,

$$\begin{aligned} &f_0 = -B(\xi), \qquad h_0 = \pi(1+\alpha_0)B(\xi),\\ &Ra_0 = \frac{\pi^2}{1+A}\frac{(1+\alpha_0)^2}{\alpha_0}, \end{aligned} \tag{C.7}$$

where the main aim here is to determine an equation for $B(\xi)$.

At $O(\lambda^{2/3})$ the following equations are obtained,

$$\pi^2(1+\alpha_0)f_1 + \pi h_1 = \ddot{f}_0 - \pi^2\alpha_1 f_0, \tag{C.8a}$$

$$\begin{aligned} &Ra_0(1+A)(h_1+\pi f_1) - \pi^2(1+\alpha_0)h_1\\ &\quad = -\ddot{h}_0 + \pi^2\alpha_1 h_0 - Ra_1(1+A)(h_0+\pi f_0), \end{aligned} \tag{C.8b}$$

which, after substitution of known expressions for f_0, h_0 and Ra_0, and after multiplication of each equation by suitable constants, yields the system,

$$\begin{aligned} &\pi^2(1+\alpha_0)h_1 + \pi^3(1+\alpha_0)^2 f_1\\ &\quad = \pi(1+\alpha_0)\Big(-\ddot{B} + \pi^2\alpha_1 B\Big), \end{aligned} \tag{C.9a}$$

$$\begin{aligned} &\pi^2(1+\alpha_0)h_1 + \pi^3(1+\alpha_0)^2 f_1\\ &\quad = \pi(1+\alpha_0)\Big(-\ddot{B} + \pi^2\alpha_1 B\Big)\alpha_0 - Ra_1(1+A)\pi\alpha_0^2 B. \end{aligned} \tag{C.9b}$$

Given that the left hand sides of these two equations are identical, it is essential that the right hand sides are also identical otherwise the system does not have a solution. Hence we find that $\alpha_0 = 1$ and $Ra_1 = 0$, and α_1 may be left unspecified at present. Acquisition of these values means that the $O(1)$ solutions are now,

$$\begin{aligned} &f_0 = -B(\xi), \qquad h_0 = 2\pi B(\xi), \qquad Ra_0 = \frac{4\pi^2}{1+A},\\ &\alpha_0 = 1, \end{aligned} \tag{C.10}$$

while the two $O(\lambda^{2/3})$ reduce to the following one equation,

$$2\pi^2 h_1 + 4\pi^3 f_1 = 2\pi\left(-\ddot{B} + \pi^2\alpha_1 B\right), \tag{C.11}$$

for which the solution may be written as,

$$\begin{aligned} f_1 &= \frac{1}{2\pi^2}\left(-\ddot{B} + \pi^2\alpha_1 B\right)(1-c), \\ h_1 &= \frac{1}{\pi}\left(-\ddot{B} + \pi^2\alpha_1 B\right)c, \end{aligned} \tag{C.12}$$

where c is an unspecified constant.

At $O(\lambda^{4/3})$ we obtain,

$$2\pi^2 f_2 + \pi h_2 = \ddot{f}_1 - \pi^2(\alpha_1 f_1 + \alpha_2 f_0), \tag{C.13a}$$

$$\begin{aligned} &4\pi^3 f_2 + 2\pi^2 h_2 = -\ddot{h}_1 + \tfrac{1}{2}Ra_0 A\xi^2(h_0 + \pi f_0) \\ &-Ra_2(1+A)(h_0 + \pi f_0) + \pi^2(\alpha_1 h_1 + \alpha_2 h_0). \end{aligned} \tag{C.13b}$$

Once more we substitute known terms and, together with the suitable multiplication of each equation, we obtain,

$$\begin{aligned} &4\pi^3 f_2 + 2\pi^2 h_2 \\ &\quad = 2\pi^3\alpha_2 B + \frac{1}{\pi}\left(\dddot{B} - 2\pi^2\alpha_1\ddot{B} + \pi^4\alpha_1^2 B\right)(c-1) \end{aligned} \tag{C.14a}$$

$$\begin{aligned} 4\pi^3 f_2 + 2\pi^2 h_2 &= 2\pi^3\alpha_2 B + \frac{1}{\pi}\left(\ddddot{B} - 2\pi^2\alpha_1\ddot{B} + \pi^4\alpha_1^2 B\right)c \\ &\quad + 2\pi^3\frac{A}{1+A}\xi^2 B - Ra_2(1+A)\pi B. \end{aligned} \tag{C.14b}$$

Once again we require the right hand sides to be identical as a solvability condition, and therefore we obtain the following equation for B,

$$\ddddot{B} - 2\pi^2\alpha_1\ddot{B} + \pi^4\alpha_1^2 B = Ra_2(1+A)\pi^2 B - 2\pi^4\frac{A}{1+A}\xi^2 B, \tag{C.15}$$

which is independent of the constant, c, and the as-yet unknown α_2. This is a fourth-order version of the second order parabolic cylinder equation and it is very similar to the one derived in Rees [13]. It forms an eigenvalue problem for Ra_2 as a function of both A and α_1. We would expect the primary mode to be even about $\xi = 0$ and to tend to zero as $\xi \to \infty$. However, it is possible to rescale this equation into one which is independent of A by making the following substitutions,

$$\begin{aligned} X &= \left(\frac{A}{1+A}\right)^{1/6}\xi, \qquad \gamma = \pi^2\left(\frac{1+A}{A}\right)^{1/3}\alpha_1, \\ S &= \pi^2 Ra_2(1+A)\left(\frac{1+A}{A}\right)^{2/3}, \end{aligned} \tag{C.16}$$

and therefore Eq. (C.15) reduces to

$$B_{XXXX} - 2\gamma B_{XX} + \gamma^2 B = -2\pi^4 X^2 B + SB. \tag{C.17}$$

This equation was solved using a fourth-order Runge–Kutta scheme in the range $0 \le X \le 5$ with 250 intervals and the solutions obtained are accurate to more than six significant figures. The eigenvalue, S, is a function of γ, and the variation is shown in Fig. 10. The minimum value is $S = 30.39795$ which arises when $\gamma = -2.532679$. Therefore we conclude that the small-λ critical values for the $v = 0$ mode are given by,

$$Ra_c = \frac{1}{1+A}\left[4\pi^2 + \frac{30.39795}{\pi^2}\left(\frac{A}{1+A}\right)^{2/3}\lambda^{4/3} + \cdots\right], \tag{C.18a}$$

$$k_c/\pi = 1 - \frac{2.532679}{2\pi^2}\left(\frac{A}{1+A}\right)^{1/3}\lambda^{2/3} + \cdots. \tag{C.18b}$$

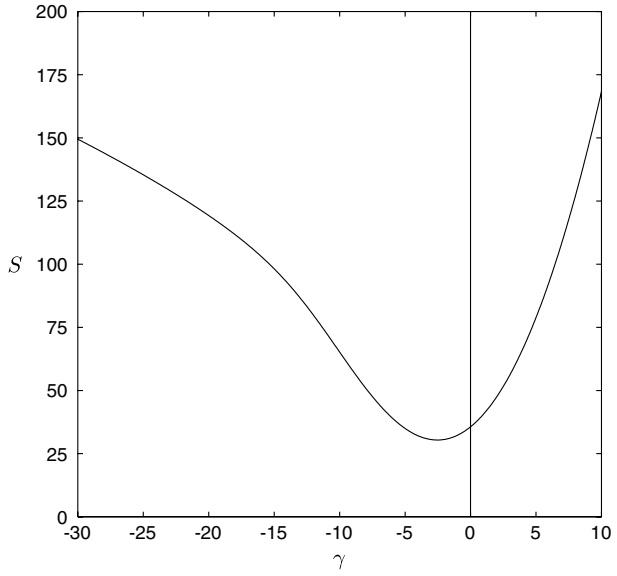

Fig. 10. The variation of the eigenvalue, S, as a function of γ.

Table 2
Comparison between the numerical critical data ($P = 5$) and the two-term asymptotic formulae for $P \gg 1$ given in Eq. (C.19).

A	Ra_c		k_c/π	
	Num	Asymp	Num	Asymp
0.1	36.663839	36.657132	0.946997	0.932817
0.2	33.998515	33.952766	0.939348	0.917774
0.3	31.654847	31.576754	0.935643	0.908353
0.4	29.596858	29.493019	0.933617	0.901591
0.5	27.781541	27.657550	0.932459	0.896402
0.6	26.171086	26.031465	0.931802	0.892254
0.7	24.734049	24.582398	0.931453	0.888842
0.8	23.444622	23.283791	0.931301	0.885976
0.9	22.281635	22.113879	0.931279	0.883528

In terms of the period, P, the equivalent expressions are,

$$\begin{aligned} &Ra_c \\ &= \frac{1}{1+A}\left[4\pi^2 + \frac{30.39795}{\pi^2}\left(\frac{A}{1+A}\right)^{2/3}\left(\frac{2\pi}{P}\right)^{4/3} + \cdots\right], \end{aligned} \tag{C.19a}$$

$$k_c/\pi = 1 - \frac{2.532679}{2\pi^2}\left(\frac{A}{1+A}\right)^{1/3}\left(\frac{2\pi}{P}\right)^{2/3} + \cdots. \tag{C.19b}$$

The asymptotic limit as $P \to \infty$ is $Ra_c = 4\pi^2/(1+A)$. The onset of convection will then be triggered locally in the planes where the permeability has its maximum value $K_{max} = (1+A)K_0$. It is quite obvious that this local convection (asymptotically for large P) will arise at a local Rayleigh number $4\pi^2$, where this local Rayleigh number is defined with K_{max} as the permeability instead of the average permeability K_0.

Comparisons between these asymptotic expressions and the accurate numerical values are given in Table 2. We see that the values for Ra_c agree to better than 0.1% throughout the range of values of A even though $P = 5$ is not a particularly large value. The comparison between the critical wavenumbers is not so good, but the series for k_c is clearly more slowly converging since the first correction to the leading order term is one which is only of $O(P^{-2/3})$.

References

[1] C.W. Horton, F.T. Rogers, Convection currents in a porous medium, J. Appl. Phys. 16 (1945) 367–370.
[2] E.R. Lapwood, Convection of a fluid in a porous medium, Proc. Cambridge Philos. Soc. 44 (1948) 508–521.

[3] D.A. Nield, A. Bejan, Convection in Porous Media, fourth ed., Springer-Verlag, New York, 2013.
[4] E. Palm, J.E. Weber, O. Kvernvold, On steady convection in a porous medium, J. Fluid Mech. 54 (1972) 153–161.
[5] R. McKibbin, M.J. O'Sullivan, Onset of convection in a layered porous medium heated from below, J. Fluid Mech. 96 (1980) 375–393.
[6] D.A.S. Rees, D.S. Riley, The three-dimensional stability of finite-amplitude convection in a layered porous medium heated from below, J. Fluid Mech. 211 (1990) 437–461.
[7] D.A. Nield, C.T. Simmons, A discussion on the effect of heterogeneity on the onset of convection in a porous medium, Transp. Porous Media 68 (2007) 413–421.
[8] R. McKibbin, Heat transfer in a vertically-layered porous medium heated from below, Transp. Porous Media 1 (1986) 361–370.
[9] D.A. Nield, Convective heat transfer in porous media with columnar structure, Transp. Porous Media 2 (1987) 177–185.
[10] A. De Wit, G.M. Homsy, Viscous fingering in periodically heterogeneous porous media. I. formulation and linear instability, J. Chem. Phys. 107 (1997) 9609–9618.
[11] A. De Wit, G.M. Homsy, Viscous fingering in periodically heterogeneous porous media. II. Numerical simulations, J. Chem. Phys. 107 (1997) 9619–9628.
[12] D.A.S. Rees, P.A. Tyvand, Onset of convection in a porous layer with continuous periodic horizontal stratification. Part I. Two-dimensional convection, Transp. Porous Media 77 (2009) 187–205.
[13] D.A.S. Rees, The effect of long-wavelength thermal modulations on the onset of convection in an infinite porous layer heated from below, Quart. J. Mech. Appl. Math. 43 (1990) 189–214.